HHS Public Access

Author manuscript

Methods Mol Biol. Author manuscript; available in PMC 2019 January 01.

Published in final edited form as:

Methods Mol Biol. 2018 ; 1749: 175–193. doi:10.1007/978-1-4939-7701-7_14.

Intravital Imaging of Tumor Cell Motility in the Tumor Microenvironment Context

Battuya Bayarmagnai[1], **Louisiane Perrin**[1], **Kamyar Esmaeili Pourfarhangi**[1], and **Bojana Gligorijevic**[1,2,*]

[1]Bioengineering department, College of Engineering, Temple University, Philadelphia, PA, 19122

[2]Cancer Biology Program, Fox Chase Cancer Center, Philadelphia, PA, 19111

Abstract

Cancer cell motility and invasion are key features of metastatic tumors. Both are highly linked to tumor microenvironmental parameters, such as collagen architecture or macrophage density. However, due to the genetic, epigenetic and microenvironmental heterogeneities, only a small portion of tumor cells in the primary tumor are motile and furthermore, only a small portion of those will metastasize. This creates a challenge in predicting metastatic fate of single cells based on the phenotype they exhibit in the primary tumor. To overcome this challenge, tumor cell subpopulations need to be monitored at several timescales, mapping their phenotype in primary tumor as well as their potential homing to the secondary tumor site. Additionally, to address the spatial heterogeneity of the tumor microenvironment and how it relates to tumor cell phenotypes, large numbers of images need to be obtained from the same tumor. Finally, as the microenvironment complexity results in nonlinear relationships between tumor cell phenotype and its surroundings, advanced statistical models are required to interpret the imaging data. Toward improving our understanding of the relationship between cancer cell motility, the tumor microenvironment context and successful metastasis, we have developed several intravital approaches for continuous and longitudinal imaging, as well as data classification via support vector machine (SVM) algorithm. We also describe methods that extend the capabilities of intravital imaging by postsacrificial microscopy of the lung as well as correlative immunofluorescence in the primary tumor.

Keywords

Tumor microenvironment; Motility; Intravital imaging; Correlative immunofluorescence; Invadopodia; Invasion; 4D multiphoton fluorescent microscopy; Second harmonic generation; Photoconvertible proteins; Support vector machine classification

*Corresponding author: bojana.gligorijevic@temple.edu.

Electronic Supplementary Material: The online version of this chapter (https://doi.org/10.1007/978-1-4939-7701-7_14) contains supplementary material, which is available to authorized users.

1 Introduction

Metastasis remains the leading cause of breast cancer-related deaths. Unlike the primary tumor, which can be managed in the clinic with chemotherapy and surgery, there is currently no effective treatment for metastasis [1]. Metastasis is a complex, multistep process, during which cancer cells dissociate from the rest of the primary tumor, move through the tissue and disseminate to secondary organs [2]. Chemical and physical cues from the tumor microenvironment, i.e. host cells [3] and the extracellular matrix (ECM) [4–6], play a significant role in shaping cancer cell behaviors related to metastasis, namely epithelial-to-mesenchymal transition (EMT), motility, invasion, homing, etc. Complex and dynamic interactions between tumor cells and the tumor microenvironment result in shifting the balance between cell behaviors accessible from the current genetic and transcriptomic landscape as well as the emergence of new cancer cell phenotypes [7, 8]. To understand such interactions at the single cell level in a quantitative fashion, it is essential to image cancer cells in real time in the context of their native niche.

With the emergence of multiphoton microscopy [9], it has become possible to study in vivo dynamic events in real time in mouse models, a notable example being intravital imaging of cancer cell motility [10]. Compared to confocal microscopy, multiphoton imaging allows deeper penetration and decreased light scattering as a result of excitation cross-sections being in the nearinfrared range of wavelengths. Furthermore, the use of femtosecond pulse lasers allows acquisition of second harmonic generated (SHG) signals, produced by noncentrosymmetric structures, including collagen I fibers abundant in most solid tumors. Unlike fluorescent signals, which need to be exogenously supplied to the sample, SHG signal is endogenous and originates from the dipole orientation of collagen fibers [11, 12].

Continuous intravital imaging in mouse models is generally limited to several hours, which allows high quality measurements of motility parameters in tumor cells as well as host immune cells [13, 14] or fibroblasts [15]. In addition, blood vessel flow and collagen architecture can be measured simultaneously. However, to fate-map specific cells or niches within the tumor, observations need to include metastatic events such as intravasation and lung colonization, which occur on a scale of days. As common intravital microscopy in tumors does not allow for freely moving animals, animals are anesthetized [16, 17] and imaging is limited to 5–24 h. Hence, longitudinal imaging [18, 19] is necessary to map the journey from primary to secondary tumor site. To ensure monitoring of the same tumor regions over multiple (static or continuous) imaging sessions, the utilization of photoconvertible fluorophores, such as Dendra2, is optimal [20, 21]. Dendra2 irreversibly switches green-to-red following 405 nm exposure, enabling us to track tumor cells longitudinally.

In this chapter we provide a guide to performing intravital imaging of cell motility in photoconvertible Dendra2-labeled breast carcinoma tissues and image analysis. We introduce the surgical procedures and lay out the steps for real-time, continuous imaging and analysis of 4-color, 4D stacks demonstrating two different motility phenotypes of tumor cells: fast- and slow-(invadopodia-driven) locomoting cells. Microenvironmental features are extracted from the same 4D stacks and finally, SVM classification identifies the

microenvironmental conditions amenable to presence of fast- or slow-locomoting cells. We describe how photoconversion can be used in vivo for longitudinal imaging of the same regions of interest. Lastly, we discuss postsacrificial approaches that can extend the capabilities of intravital imaging of lung metastases and correlative immunofluorescence of the primary tumor sections.

2 Materials

2.1 Intravital Imaging and Photoconversion

1. Mouse strains:
   a. *MMTV-PyMT* × *MMTV-iCre/CAG-CAC-Dendra2* (cytoplasm of all tumor cells labeled with photoconvertible Dendra2).
   b. *MMTV-PyMT* × *MMTV-iCre/CAG-CAC-Dendra2* × *c-fms-CFP* (cytoplasm of all tumor cells and macrophages labeled).
   c. MDA-MB-231-Dendra2 cells orthotopically injected into SCID mice.
2. Olympus FV1200MPE multiphoton laser scanning microscope.
3. UPLSAPO 30× objective with silicone oil immersion, NA 1.05.
4. ThorLabs PM200 Handheld optical power and energy meter.
5. Temperature control environmental chamber.
6. Infrared heating pad.
7. Isoflurane.
8. Anesthesia mask.
9. Surgical drape.
10. Tissue forceps.
11. Micro scissors.
12. Trimmer.
13. Ocular lubricant ointment.
14. 70% ethanol.
15. Sterile 1× PBS Dulbecco’s phosphate-buffered saline (1× PBS).
16. Dextran, Texas Red, 70 kDa (Molecular Probes).
17. MMPSense 680 Fluorescent Imaging Agent (PerkinElmer).
18. Transfer pipettes.
19. Cotton-tipped applicators.
20. Insulin syringe.
21. Super glue liquid, longneck bottle.

22. Labeling tape.

2.2 Immunofluorescence

1. 1× Dulbecco's phosphate-buffered saline (1× PBS).
2. Fixative: 4% paraformaldehyde, 1× PBS.
3. O.C.T. (optimal cutting temperature) Compound.
4. 30% w/v sucrose solution.
5. Isopentane (2-methylbutane).
6. Dry ice.
7. Disposable cryomolds.
8. Positively charged microscope glass slides.
9. Blocking Solution: 1% bovine serum albumin (BSA), 1% fetal bovine serum (FBS), 1× PBS.
10. Liquid Blocker Super Pap Pen.
11. Permeabilization Solution: 0.1% Triton X-100, 1× PBS.
12. Acetone.
13. Antibodies and fluorescent dyes: Anti-Ki67 (Abcam, cat. abcam15580, 1:200), Anti-fibronectin (Abcam, cat. ab6328, 1:100), Phalloidin conjugated to Alexa Fluor 633.
14. Fluoromount-G mounting medium.
15. Cover glass.
16. Nail polish.

3 Methods

3.1 Surgical Preparation

The animals must be surgically prepared for imaging by removing skin and exposing the cells to be imaged. Here, we briefly describe the mammary skin flap procedure, which is suitable for continuous imaging. For the skin flap preparation, the mammary tumor tissue of the fourth inguinal mammary gland is separated from the peritoneum on a skin flap (Fig. 1a). The fourth inguinal mammary gland is sufficiently distant from the chest area, which is most heavily affected by breathing. Separation from the body with the skin flap further reduces breathing disturbance on imaging. This approach is technically simple and is suitable for short, one-time imaging sessions only. The imaging time is limited to generally 6–8 h due to inflammation and blood vessel damage as a result of prolonged exposure of the tissue to the outside environment. This duration can be increased to 24 h with careful monitoring of vital signs [18, 23]. Repeated imaging is not advised and the animal is commonly sacrificed after imaging.

In the event that repeated longitudinal imaging is desired, mammary imaging window preparation is more appropriate (Fig. 1a). The imaging window, which consists of a glass coverslip on top of a plastic or a metal ring [19, 24], is sutured into the skin on top of the tumor tissue. The animal is allowed to heal for 3 days, after which it is available for continuous, noninvasive imaging and daily, longitudinal monitoring. The advantage of this approach is the prolonged monitoring (up to 21 days) of a developing tumor. With additional points of reference (photoconvertible fluoro-phores, fluorescent microbeads, photo-tattoo [25]), which can be used to monitor the same region of interest. However, this method requires additional surgery training for personnel and a three-day post surgery recovery time for the animal.

3.2 Labeling Blood Vessels and/or Macrophages

Intravenous, tail vein injection of 70/155 kDa fluorescent dextran (100 μg) will label active blood vessels [26]. 2–6 h following injection, the 70 kDa probe will extravasate and label the phagocytic subpopulation of macrophages [27]. For imaging total macrophage population, using transgenic mouse models is advised [23, 28] (*see* Subheading 2.1, **item 1**). Note that macrophage labeling will remain present for 5–7 days.

3.3 Image Acquisition

1. The animal is placed in an environmental chamber at 37 °C with continuous 1.5% isoflurane flow for the maintenance of anesthesia. 50 μL of sterile 1× PBS is administered intravenously (tail vein) every hour for hydration.
2. Locate a region of interest in the primary tumor, characterized by the presence of flowing blood vessels and bright fluorescence signal. Avoid areas rich in adipocytes as they scatter excitation light and obstruct fluorescence (Fig. 1b, c).
3. Acquire 4D stacks for the duration of interest (generally 30–60 min).
4. If longitudinal imaging of the acquired area is needed, proceed to photoconverting regions of interest (Subheading 3.8).

3.4 Detection and Quantification of Fast-Locomoting Cells

Translocating or motile cells are characterized by the extension of the cell front, movement of the center and the contraction of the rear.

1. Open a 4D stack in ImageJ.
2. Correct for movement by running HyperStackReg plugin to align sections in XY plane [29].
3. Visually score each z-section of the 4D stack movies for the morphological determinants of tumor cell fast locomotion. For the ease of processing, field of view (FOV) can be divided into smaller (1/4) sections (Fig. 2a, left panels). Select one z-section for further analysis.
4. Subtract frame taken at time 0 from the frame taken at time 60 min (*Process > Image Calculator > Subtract images*). Acquire an image with all pixels

translocated during the time period. This step can be performed for differences between any two time points (Fig. 2a, middle panels).

5. Threshold the image to remove background fluorescence (*Image > Adjust > Threshold*).

6. Using Particle Analysis plugin in ImageJ, count the number of locomoting cells and obtain the mask of cell translocation. By adjusting the values for particle size and circularity, false positives, such as cell edges due to XY shift attributed to breathing artifacts, can be removed (Fig. 2a, right panels) (*Analyze > Analyze Particles > Size (15 μm^2-infinity), Circularity (0.1–1)*).

7. Compare the mask with the 4D stack and ensure that all locomoting cells have been captured.

8. If not all locomoting cells are captured, readjust values for size and circularity in the Particle Analysis tool.

9. Manually remove remaining false positives, such as cell edges due to motion artifacts (Draw ROI *> Edit > Fill*).

10. Run Particle Analysis tool on the final processed image to obtain the count of locomoting cells.

11. Merge the obtained mask of locomoting cells with the frame at time 0 to visualize initial tumor cell position and track of movement (*Image > Color > Merge Channels*).

3.5 Detection and Quantification of Invadopodia in Slow-Locomoting Cells

Invadopodia are highly dynamic, small protrusions on the surface of tumor cells, characterized by finger-like morphology, <3 μm wide and <7 μm in length, and extension/retraction cycles. In vivo, invadopodia go through extension and retraction cycles of 3–20 min [30, 31], as well as change the position of the growing tip, making the selective identification via motility analysis possible. Importantly, only the cells exhibiting invadopodia-driven slow locomotion phenotype will successfully metastasize to the lung [31, 32].

1. Open a 4D stack in ImageJ.

2. Correct for movement by running HyperStackReg plugin to align sections in XY plane [29].

3. Visually score each z-section of the 4D stack movies at 2–4× zoom for the morphological determinants of tumor cells with invadopodia. For the ease of processing, cells can be analyzed individually (Fig. 2b).

4. Subtract frame taken at time 0 from the frame taken at 3 min to 15 min (*Process > Image Calculator > Subtract images*) (*see* **Note 1**). Acquire an image with all pixels translocated during the time period.

5. Threshold the image to remove background fluorescence (*Image > Adjust > Threshold*).

6. Using Particle Analysis, count the number of invadopodia per cell and obtain the mask of the dynamics of invadopodia over the time period. By adjusting the values for particle size and circularity, one can remove false positives such as cell edges due to XY shift (*Analyze > Analyze Particles > Size (0.5 μm^2-infinity), Circularity (0–1)*).
7. Compare the mask with the 4D stack and ensure that all invadopodia have been captured.
8. If not all invadopodia are captured, readjust values for size and circularity in the Particle Analysis tool.
9. Manually remove remaining false positives (Draw ROI *> Edit > Fill*).
10. Run Particle Analysis tool on the final processed image to obtain the count of invadopodia.
11. Overlay the obtained mask of translocated protrusions with the frame at time 0 to visualize the extension/retraction of invadopodia (*Image > Color > Merge Channels*) (Fig. 2b).
12. Migration of the entire tumor cell body of invadopodia-driven slow-locomoting cells can be captured by extending the time-lapse imaging to 5–8 h.

3.6 Analysis of the In Vivo Microenvironmental Parameters

Features we routinely monitor in the tumor microenvironment include the density of collagen fibers, tumor cells and phagocytic macrophages, as well as the number and diameter of flowing blood vessels present in the FOV. Directionality and alignment of collagen fibers [33] and speed of blood vessel flow [34] can also be incorporated into the analysis without additional labeling. In animals where total macrophage population is labeled via *c-fms* promoter (*see* Subheading 2.1, **item 1a**), the number and speed of (non)phagocytic macrophages can also be quantified. Finally, the amount of degraded ECM can be measured via the injection of the protease-activatable imaging probe MMPSense 680, whose fluorescence increases >10-fold following proteolysis by key matrix metalloproteinases (MMP-2, -3, -9, and -13) [31].

1. Open a multicolor 4D stack in ImageJ.
2. Z project all frames using the maximal intensity mode (*Image > Stacks > Z Project*).
3. Visually score the entire 4D hyperstack and duplicate the 3D, 4-color stack at first time point (*see* **Note 2**) (Fig. 1c).
4. Separate channels and apply a smoothing filter (*Process > Smooth*). To measure collagen fiber alignment, save the image corresponding to the collagen channel using ".tiff" format and follow **steps 10**–**14**.
5. Threshold each channel to remove background fluorescence (*Image > Adjust > Threshold*) (*see* **Note 3**) and obtain binary images for each parameter (Fig. 2c).

6. Measure the density of collagen fibers and tumor cells, defined as the percent area above threshold in each corresponding channel (enable the function “Limit to threshold” under *Analyze > Set Measurements*).

7. Separate macrophages from blood vessels on the basis of size and morphology in the dextran channel (*Analyze > Analyze Particles*).

8. Determine the number of flowing blood vessels and measure the diameter of the largest flowing blood vessel visible in the FOV using the “Straight Line” tool.

9. Manually count the number or measure the density of macrophages labeled with 70 kDa dextran in the FOV.

10. To measure collagen fiber alignment, import the image saved in **step 4** to ctFIRE software [33] (*Import image/data*) (*see* **Note 4**).

11. Optimize the accuracy of fiber detection by adjusting the parameters (*see* **Note 5**).

12. Run fiber detection analysis. The nonoverlaid and the reconstructed images are displayed (Fig. 2c′). If the overlaid fiber map shows non-negligible errors in fiber detection, click on the *Reset* button and adjust the detection parameters (**step 11**).

13. When fiber detection is satisfactory, check “Straightness histogram & values” and “Angle histrogram & values” under section “Select Output,” and run the postprocessing analysis (*see* **Note 6**), which will return the histograms for Straightness (Fig. 2c′) and Angle (not shown).

14. Use the corresponding data set created in the output folder “…\ctFIREout” under the working directory to compute the average alignment of the collagen fibers in each direction.

15. Select the *Reset* button to import a new image.

3.7 Support Vector Machine Classifications

To determine the range of microenvironmental parameters amenable to fast- versus slow-motility phenotypes, SVM classification is used [35]. SVM is a supervised learning model, which constructs hyperplanes in high-dimensional spaces [36] that are nonlinearly related to the input. Depending on the complexity of the input data, the hyperplane can be as simple as a line dividing a two- dimensional space into two regions, or as complicated as a set of multidimensional nonlinear planes dividing the space into multiple zones. The discrete regions created by hyperplane(s) represent distinct classes that SVM recognizes among the input data. SVM algorithms are available for many mathematical packages, including Rstudio which is freely available. In this work, a nonlinear SVM from R-package “e-1072” [36] is used for data classification.

The source code (MotilityClassifier.R) for data classification is provided for download as a Supplementary File. The code receives the input data as a tab delimited text file and creates a SVM model with a “radial” kernel vector. Within the code, the details of each step are

provided as comments. Briefly, the code randomly selects 90% of the input data for the learning process, based on which it generates a SVM model. The model is further tuned by iterative changing of the "cost" and "gamma" values until the "bestmodel" with the least error is achieved. Using this model, the code predicts the motility phenotype of the remaining 10% of the data and prints a table reporting the precision of the classification by indicating the percentage of misclassified data (green spheres, Fig. 2d). A low misclassification percentage (<5% in Fig. 2d) means that the input variables of two classes are statistically different and can be used for predicting the type of cell motility.

3.8 Photoconversion for Longitudinal Intravital Imaging

3.8.1 Determining Optimal Photoconversion Settings

1. Using the optical power meter, measure the power level of the 405 nm laser that enters the sample.
2. Define a range to test between 0 and 600 μW (Fig. 3a). In this case, the power settings are 20% (1 μW), 30% (4 μW), 40% (64 μW), and 50% (520 μW).
3. Balance the intensities of green to the background of red in a nonsequential scan before photoconverting.
4. Open "Live Plot" window to track the fluorescence intensities of red and green channels.
5. In Time Scan window, set Interval to "Free Run" and Number to "20."
6. Set the 405 nm laser to the power level being tested and start scanning. Monitor the Live Plot window and stop scanning as soon as red fluorescence intensity hits a plateau or green fluorescence intensity drops (photobleaching).
7. Out of four settings tested, 20% (1 μW) and 30% (4 μW) laser powers are too weak to induce photoconversion (Fig. 3b′, b″). 40% (64 μW) laser power is optimal with efficient photoconversion and with minimal photobleaching of the green fluorescence (Fig. 3b, b″). 50% (520 μW) laser power is too strong and results in complete photobleaching of the fluorescent signal (Fig. 3b, b″).

3.8.2 Photoconversion of Tumor Cells In Vivo—After continuous imaging of the region of interest, decide on the area to be photoconverted

1. For a single cell, select the Point tool and place it at the center of the cell.
2. Using the optimal settings determined in Subheading 3.8.1 (64 μW laser power), scan until red fluorescence signal plateaus.
3. The photoconverted proteins diffuse and fill the entire cell (Fig. 3c, top left panel).
4. For a single area, use the selection tool to draw a rectangular region of interest (*see* **Note 7**) and scan (Fig. 3c, top right panel).

5. For photoconverting several regions (Fig. 3c, bottom left panel) or all cells in that field of view (FOV) (Fig. 3c, bottom right panel, *see* **Note 8**) the same tool as in **step 4** can be used (*see* **Note 9**).

6. Using photoconverted regions as tissue landmarks, the same FOV can be located at multiple imaging sessions, allowing longitudinal imaging of tumor cells and/or microenvironmental parameters (Fig. 3d).

3.9 Ex Vivo Imaging of Lung Metastases

Breast cancers commonly metastasize to the lung, liver, brain, and bone. Likewise, in our mouse models, we observe single cells and micrometastases in the lung. Counting the number of single cells and colonies is suitable for assessing total number of metastases following euthanasia of the animal at the end of imaging. Additionally, the number of red metastases can be measured at a set time point (2–7 days) following photoconversion, enabling the measurement of dynamics of tumor cell homing, proliferation, or dormancy [37] in the lung. Dendra2 red variant is highly stable and protein turnover in vivo is negligible ([21, 24]; therefore, with each cell division red fluorescence is diluted by 50%. As the non-photoconverted green variant of Dendra2 is continuously being synthesized under the CMV promoter, cells will become orange and yellow following cell division(s) (Fig. 4a′). The origin of green cells cannot be delineated, as they can be both descending from yellow cells, or arriving from the nonphotoconverted green regions of the primary tumor.

1. Immediately after sacrificing, secure the mouse in supine position by taping the legs to the surgical surface.

2. Make a midline incision on the chest, open the skin and peritoneum, exposing the ribcage.

3. Cut through the bones and cartilage to open up the ribcage. Absorb blood with tissue paper.

4. Harvest the lung tissue and transfer it to a dish with 1× PBS.

5. Separate two lobes of the lung and quickly rinse with fresh 1× PBS.

6. In a drop of 1× PBS, transfer the lung to a coverslip or a glass-bottom microscope dish for imaging.

7. Image metastatic lesions in 20 random FOV (Fig. 4a).

8. Using image processing, quantify the number of metastases:

    a. Open image in ImageJ.

    b. Remove background fluorescence and set threshold (*Image > Adjust > Threshold*).

    c. Count the number of cells (*Analyze > Analyze Particles > Size (15 μm^2-infinity), Circularity (0.1–1)*).

3.10 Correlative Immunofluorescence

1. After imaging and photoconversion, harvest the tumor tissue and immediately fix in 4% paraformaldehyde solution for 1 h at room temperature and then overnight at 4 °C.
2. Wash the tissue in cold 1× PBS for 1 h at 4 °C.
3. Incubate tissue in 30% sucrose solution overnight at 4 °C.
4. In a cryomold, immerse the tumor tissue in O.C.T compound, orient it and freeze it in an isopentane bath (*see* **Note 10**).
5. The frozen tissue can be stored at −80 °C until ready to be sectioned.
6. Using a cryostat, section the tissue sample into 6–10 μm thick slices and mount onto positively charged microscope glass slides.
7. The slides can be stored at −80 °C until ready to be stained.
8. Wash off O.C.T. compound from tissue sections by repeatedly dipping slides in water.
9. To permeabilize tissue sections, immerse slides in permeabilization solution for 10 min. Alternatively, sections can be permeabilized for 10 min in ice-cold acetone (procedure we use for labeling microenvironmental parameters, such as endomucin, laminin, collagen IV, collagen I, or fibronectin).
10. Briefly air-dry slides.
11. Draw a circle around each tissue section with a liquid blocker pen to provide a barrier for solutions.
12. Block tissues with 50–100 μL drops of the blocking solution for 2 h at room temperature. Alternatively, block tissues overnight at 4 °C. To prevent evaporation, place slides into a humidified chamber.
13. Incubate with primary antibodies diluted to appropriate concentrations in 50–100 μL of blocking solution for 3 h at room temperature, in a humidified chamber.
14. Wash by dipping slides in 1× PBS.
15. Incubate with secondary antibodies and DAPI diluted in 50–100 μL of blocking solution for 2 h at room temperature in a humidified chamber and protected from light.
16. Wash by dipping slides in 1× PBS.
17. Briefly air-dry slides.
18. Place a drop of Fluoromount-G on each tissue section.
19. Avoiding air bubbles, place a glass coverslip and seal with nail polish.
20. The glass slides with tissue sections can be stored at 4 °C and protected from light, until ready to be imaged.

21. Image cryosections (Fig. 4b–e).

4 Notes

1. The choice of time points for invadopodia analysis depends on the frequency of extension–retraction cycles.
2. Identify a time-point when all microenvironmental parameters of interest are clearly visible. For example, to visualize blood vessels, it is advised to start imaging immediately after injection of fluorescent dextran. For phagocytic macrophages, inject the animal with fluorescent dextran >3 h prior to the imaging session. Both blood vessels and macrophages will be visible in the time window of 1–3 h following injection.
3. For the first set of images in the series, suitable threshold value is set manually. At that time, users can decide on a satisfactory automated thresholding method (*Image > Adjust > Auto Threshold* drop down list). The threshold value will need to be adjusted for each imaging session if the acquisition parameters differ.
4. The ctFIRE software requires MATLAB compiler runtime (MCR 7.17 2012a) installation.
5. A description of each parameter can be found in the User Manual (available at http://loci.wisc.edu/software/ctfire). We recommend starting with default values. The parameters and the options under the sections “Output Figure Control” and “Select Output” can be modified after fiber detection, during the postprocessing step (*see* **step 13**).
6. Additional outputs can be selected: “Overlaid fibers,” “Non-overlaid fibers,” “Angle histogram & values,” “Length histogram & values,” and/or “Width histogram & values.”
7. Areas containing >20 cells are easier to locate later in cryosections and determine the orientation of the tissue.
8. Photoconverting all four corners of the FOV is a useful method if one plans to perform correlative immunofluorescence. This way, the FOV can be located by the photoconverted corners, while leaving the rest of the FOV available for labeling in the red channel. Photoconversion of the entire FOV is useful if the number of photoconverted cells needs to be maximized, such as postsacrificial imaging of lung metastases.
9. Alternatively, all cells in the FOV can be photoconverted using the mercury or LED lamp excitation through the DAPI filter [38]. Locate the area of interest and expose it to the lamp on full power for 5–10 min. This method yields photoconverted FOV with diffuse edges. If an area larger than a single FOV is needed, custom-built LED array can be used to expose the entire surface under the mammary imaging window to 405 nm light [24, 31].

10. To prepare the isopentane bath, fill a stainless steel container with isopentane and place it in dry ice. Drop a few pellets of dry ice into isopentane and wait for the boiling to stop. At this time isopentane is chilled to about −90 °C and is ready for freezing the sample. Slowly lower the sample and drop it in the isopentane bath. Leave it until the entire block is frozen through and the sample sinks to the bottom of the isopentane bath.

Supplementary Material

Refer to Web version on PubMed Central for supplementary material.

Acknowledgments

We thank Dr. Aviv Bergman for his contribution in establishing the SVM algorithm for classification. This work was supported by grants from the NIH 5K99CA172360 and Concern Foundation Award to B.G.

References

1. Steeg PS. Targeting metastasis. Nat Rev Cancer. 2016; 16:201–218. https://doi.org/10.1038/nrc.2016.25. [PubMed: 27009393]
2. Vanharanta S, Massagué J. Origins of metastatic traits. Cancer Cell. 2013; 24:410–421. https://doi.org/10.1016/j.ccr.2013.09.007. [PubMed: 24135279]
3. Quail DF, Joyce JA. Microenvironmental regulation of tumor progression and metastasis. Nat Med. 2013; 19:1423–1437. https://doi.org/10.1038/nm.3394. [PubMed: 24202395]
4. Conklin MW, Eickhoff JC, Riching KM, et al. Aligned collagen is a prognostic signature for survival in human breast carcinoma. Am J Pathol. 2011; 178:1221–1232. https://doi.org/10.1016/j.ajpath.2010.11.076. [PubMed: 21356373]
5. Gehler S, Ponik SM, Riching KM, Keely PJ. Bi-directional signaling: extracellular matrix and integrin regulation of breast tumor progression. Crit Rev Eukaryot Gene Expr. 2013; 23:139–157. [PubMed: 23582036]
6. Levental KR, Yu H, Kass L, et al. Matrix crosslinking forces tumor progression by enhancing integrin signaling. Cell. 2009; 139:891–906. https://doi.org/10.1016/j.cell.2009.10.027. [PubMed: 19931152]
7. Marusyk A, Almendro V, Polyak K. Intra-tumour heterogeneity: a looking glass for cancer? Nat Rev Cancer. 2012; 12:323–334. https://doi.org/10.1038/nrc3261. [PubMed: 22513401]
8. Bergman A, Condeelis JS, Gligorijevic B. Invadopodia in context. Cell Adhes Migr. 2014; 8:273–279. https://doi.org/10.4161/cam.28349.
9. Denk W, Strickler J, Webb W. Two-photon laser scanning fluorescence microscopy. Science. 1990; 248:73–76. https://doi.org/10.1126/science.2321027. [PubMed: 2321027]
10. Condeelis J, Segall JE. Intravital imaging of cell movement in tumours. Nat Rev Cancer. 2003; 3:921–930. https://doi.org/10.1038/nrc1231. [PubMed: 14737122]
11. Mohler W, Millard AC, Campagnola PJ. Second harmonic generation imaging of endogenous structural proteins. Methods. 2003; 29:97–109. [PubMed: 12543075]
12. Zipfel WR, Williams RM, Christie R, et al. Live tissue intrinsic emission microscopy using multiphoton-excited native fluorescence and second harmonic generation. Proc Natl Acad Sci. 2003; 100:7075–7080. https://doi.org/10.1073/pnas.0832308100. [PubMed: 12756303]
13. Li JL, Goh CC, Keeble JL, et al. Intravital multiphoton imaging of immune responses in the mouse ear skin. Nat Protoc. 2012; 7:221–234. https://doi.org/10.1038/nprot.2011.438. [PubMed: 22240584]
14. Lelkes E, Headley MB, Thornton EE, et al. The spatiotemporal cellular dynamics of lung immunity. Trends Immunol. 2014; 35:379–386. https://doi.org/10.1016/j.it.2014.05.005. [PubMed: 24974157]

15. Hirata E, Girotti MR, Viros A, et al. Intravital imaging reveals how BRAF inhibition generates drug-tolerant microenvironments with high integrin β1/FAK signaling. Cancer Cell. 2015; 27:574–588. https://doi.org/10.1016/j.ccell.2015.03.008. [PubMed: 25873177]
16. Helmchen F, Fee MS, Tank DW, Denk W. A miniature head-mounted two-photon microscope. Neuron. 2001; 31:903–912. https://doi.org/10.1016/s0896-6273(01)00421-4. [PubMed: 11580892]
17. Ghosh KK, Burns LD, Cocker ED, et al. Miniaturized integration of a fluorescence microscope. Nat Methods. 2011; 8:871–878. https://doi.org/10.1038/nmeth.1694. [PubMed: 21909102]
18. Ewald AJ, Werb Z, Egeblad M. Dynamic, long-term in vivo imaging of tumor-stroma interactions in mouse models of breast cancer using spinning-disk confocal microscopy. Cold Spring Harb Protoc. 2011; 2011:pdb.top97. https://doi.org/10.1101/pdb.top97. [PubMed: 21285277]
19. Alieva M, Ritsma L, Giedt RJ, et al. Imaging windows for long-term intravital imaging. Intravital. 2014; 3:e29917–e29916. https://doi.org/10.4161/intv.29917. [PubMed: 28243510]
20. Gurskaya NG, Verkhusha VV, Shcheglov AS, et al. Engineering of a monomeric green-to-red photoactivatable fluorescent protein induced by blue light. Nat Biotechnol. 2006; 24:461–465. https://doi.org/10.1038/nbt1191. [PubMed: 16550175]
21. Chudakov DM, Lukyanov S, Lukyanov KA. Tracking intracellular protein movements using photoswitchable fluorescent proteins PS-CFP2 and Dendra2. Nat Protoc. 2007; 2:2024–2032. https://doi.org/10.1038/nprot.2007.291. [PubMed: 17703215]
22. Génot E, Gligorijevic B. Invadosomes in their natural habitat. Eur J Cell Biol. 2014; 93:367–379. https://doi.org/10.1016/j.ejcb.2014.10.002. [PubMed: 25457677]
23. Egeblad M, Ewald AJ, Askautrud HA, et al. Visualizing stromal cell dynamics in different tumor microenvironments by spinning disk confocal microscopy. Dis Model Mech. 2008; 1:155–167. https://doi.org/10.1242/dmm.000596. [PubMed: 19048079]
24. Kedrin D, Gligorijevic B, Wyckoff J, et al. Intravital imaging of metastatic behavior through a mammary imaging window. Nat Methods. 2008; 5:1019–1021. https://doi.org/10.1038/nmeth.1269. [PubMed: 18997781]
25. Ritsma L, Vrisekoop N, van Rheenen J. In vivo imaging and histochemistry are combined in the cryosection labelling and intravital microscopy technique. Nat Commun. 2013; 4:2366. https://doi.org/10.1038/ncomms3366. [PubMed: 23978961]
26. Harney AS, Arwert EN, Entenberg D, et al. Real-time imaging reveals local, transient vascular permeability, and tumor cell Intravasation stimulated by TIE2hi macrophage- derived VEGFA. Cancer Discov. 2015; 5:932–943. https://doi.org/10.1158/2159-8290.CD-15-0012. [PubMed: 26269515]
27. Wyckoff J, Wang W, Lin EY, et al. A paracrine loop between tumor cells and macrophages is required for tumor cell migration in mammary tumors. Cancer Res. 2004; 64:7022–7029. https://doi.org/10.1158/0008-5472.CAN-04-1449. [PubMed: 15466195]
28. Wyckoff J, Gligorijevic B, Entenberg D, et al. High-resolution multiphoton imaging of tumors in vivo. Cold Spring Harb Protoc. 2011; 2011:pdb.top065904. https://doi.org/10.1101/pdb.top065904. [PubMed: 21969629]
29. Thevenaz P, Ruttimann UE, Unser M. A pyramid approach to subpixel registration based on intensity. IEEE Trans Image Process. 1998; 7:27–41. https://doi.org/10.1109/83.650848. [PubMed: 18267377]
30. Oser M, Mader CC, Gil-Henn H, et al. Specific tyrosine phosphorylation sites on cortactin regulate Nck1-dependent actin polymerization in invadopodia. J Cell Sci. 2010; 123:3662–3673. https://doi.org/10.1242/jcs.068163. [PubMed: 20971703]
31. Gligorijevic B, Bergman A, Condeelis J. Multiparametric classification links tumor microenvironments with tumor cell phenotype. PLoS Biol. 2014; 12:e1001995. https://doi.org/10.1371/journal.pbio.1001995. [PubMed: 25386698]
32. Gligorijevic B, Wyckoff J, Yamaguchi H, et al. N-WASP-mediated invadopodium formation is involved in intravasation and lung metastasis of mammary tumors. J Cell Sci. 2012; 125:724–734. https://doi.org/10.1242/jcs.092726. [PubMed: 22389406]
33. Bredfeldt JS, Liu Y, Conklin MW, et al. Automated quantification of aligned collagen for human breast carcinoma prognosis. J Pathol Inform. 2014; 5:28. https://doi.org/10.4103/2153-3539.139707. [PubMed: 25250186]

34. Dasari, S., Weber, P., Makhloufi, C., et al. Intravital microscopy imaging of the liver following Leishmania infection: an assessment of hepatic hemodynamics; J Vis Esp. 2015. p. e52303doi:https://doi.org/10.3791/52303

35. Vapnik VN. An overview of statistical learning theory. IEEE Trans Neural Netw. 1999; 10:988–999. https://doi.org/10.1109/72.788640. [PubMed: 18252602]

36. Karatzoglou A, Meyer D, Hornik K. Support vector machines in ddR. J Stat Softw. 2006; 15 https://doi.org/10.18637/jss.v015.i09.

37. Fluegen G, Avivar-Valderas A, Wang Y, et al. Phenotypic heterogeneity of disseminated tumour cells is preset by primary tumour hypoxic microenvironments. Nat Cell Biol. 2017; 19:120–132. https://doi.org/10.1038/ncb3465. [PubMed: 28114271]

38. Baker SM, Buckheit RW, Falk MM. Green-to-red photoconvertible fluorescent proteins: tracking cell and protein dynamics on standard wide-field mercury arc-based microscopes. BMC Cell Biol. 2010; 11:15. https://doi. org/10.1186/1471-2121-11-15. [PubMed: 20175925]

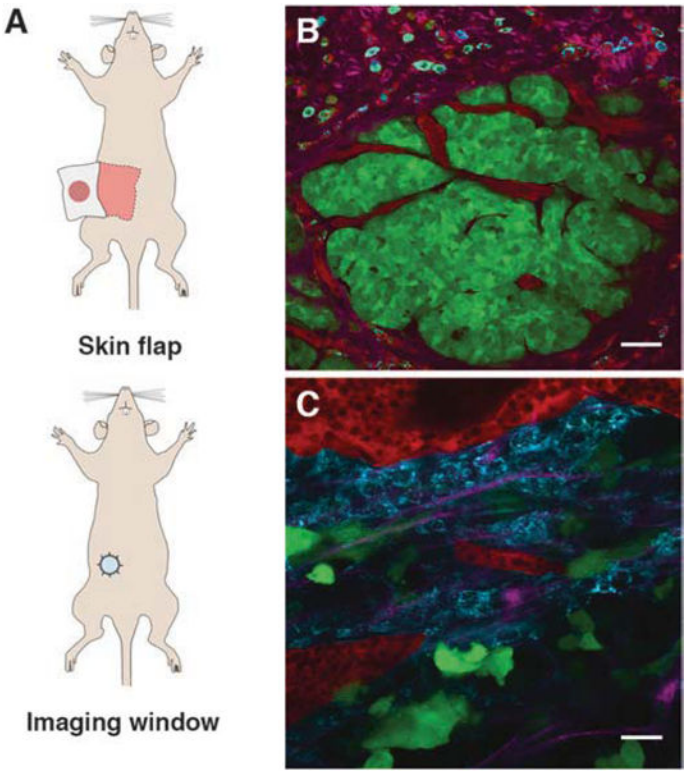

Fig. 1.

Surgical preparation and intravital images of the tumor microenvironment in transgenic and orthotopic xenograft mouse models of breast carcinoma. (**a**) Surgical preparations of mice for intravital imaging: skin flap (top) and mammary imaging window (bottom). (**b**) Intravital image of tumor cells and the surrounding tumor microenvironment in carcinoma stage of the *MMTV-PyMT × MMTV-iCre/CAGCAC-Dendra2* transgenic mouse at 13 weeks. Tumor cells (green), blood vessels (red), collagen fibers (magenta), macrophages (cyan). Scale bar 50 μm. The image is reprinted with permission from [22]. (**c**) Intravital image of tumor cells and the surrounding microenvironment in the orthotopic xenografts of MDA-MB-231-Dendra2 cells. Tumor cells (green), blood vessels (red), collagen fibers (magenta), macrophages (cyan). Scale bar 25 μm

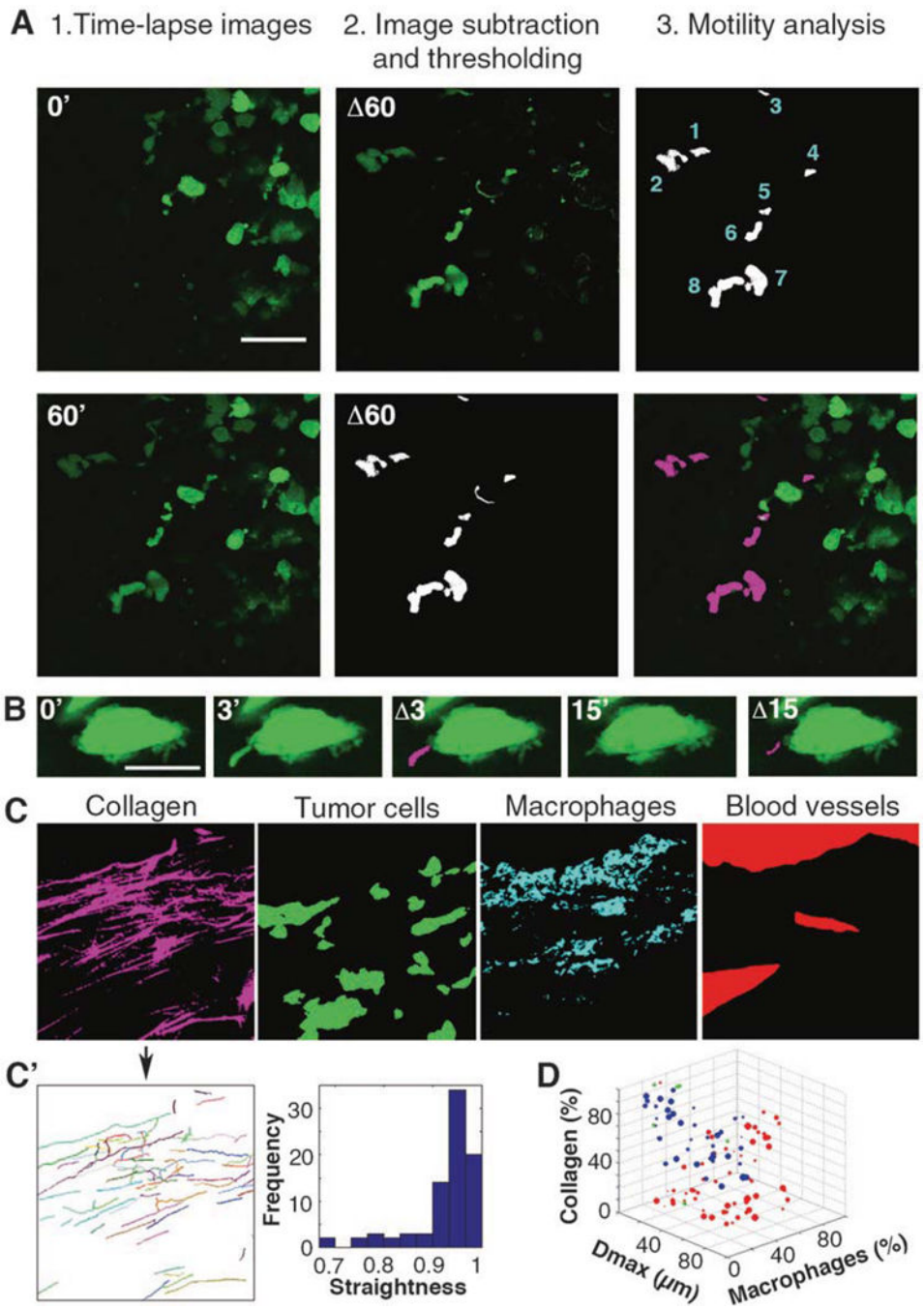

Fig. 2.

Intravital Systems Microscopy: Multiparametric SVM classification of tumor cell locomotion and microenvironmental parameters (**a**) Identifying and quantifying fast-locomoting cells. Left panels, raw images of an individual z-section from the 4D stack (at 0 and 60 min; 0′ and 60′). Middle panels, 0′ was subtracted from 60′, resulting in Δ60 (top); image was then thresholded/binarized (bottom). Right panels, results of motility analysis including quantification of fast locomoting cells (top) and the overlay with the 0′ image (bottom). Scale bar 50 μm. (**b**) Identifying and quantifying invadopodia in slow locomoting

cells. Raw images of a cell at time 0, with fully extended invadopodium at 3 min and partially retracted invadopodium at 15 min. Overlays Δ3 and Δ15 show invadopodia extension highlighted in magenta. Scale bar 10 μm. (**c**) Binarized images used for extraction of microenvironmental parameters. Image in Fig. 1c was separated and thresholded, resulting in binary images of collagen (magenta), tumor cells (green), macrophages (cyan) and blood vessels (red). (**c′**) Collagen fiber map (left) and dimensionless straightness histogram (right) from ctFIRE software. (**d**) 3D projection of SVM classification results. Red spheres denote slow locomotion, blue-fast locomotion, green- misclassifications. The size of the spheres indicates the number of locomoting cells in the FOV. D_{max} (μm) stands for the diameter of the largest blood vessel in the FOV, macrophages (%) and collagen (%) stand for the thresholded area in respective channels

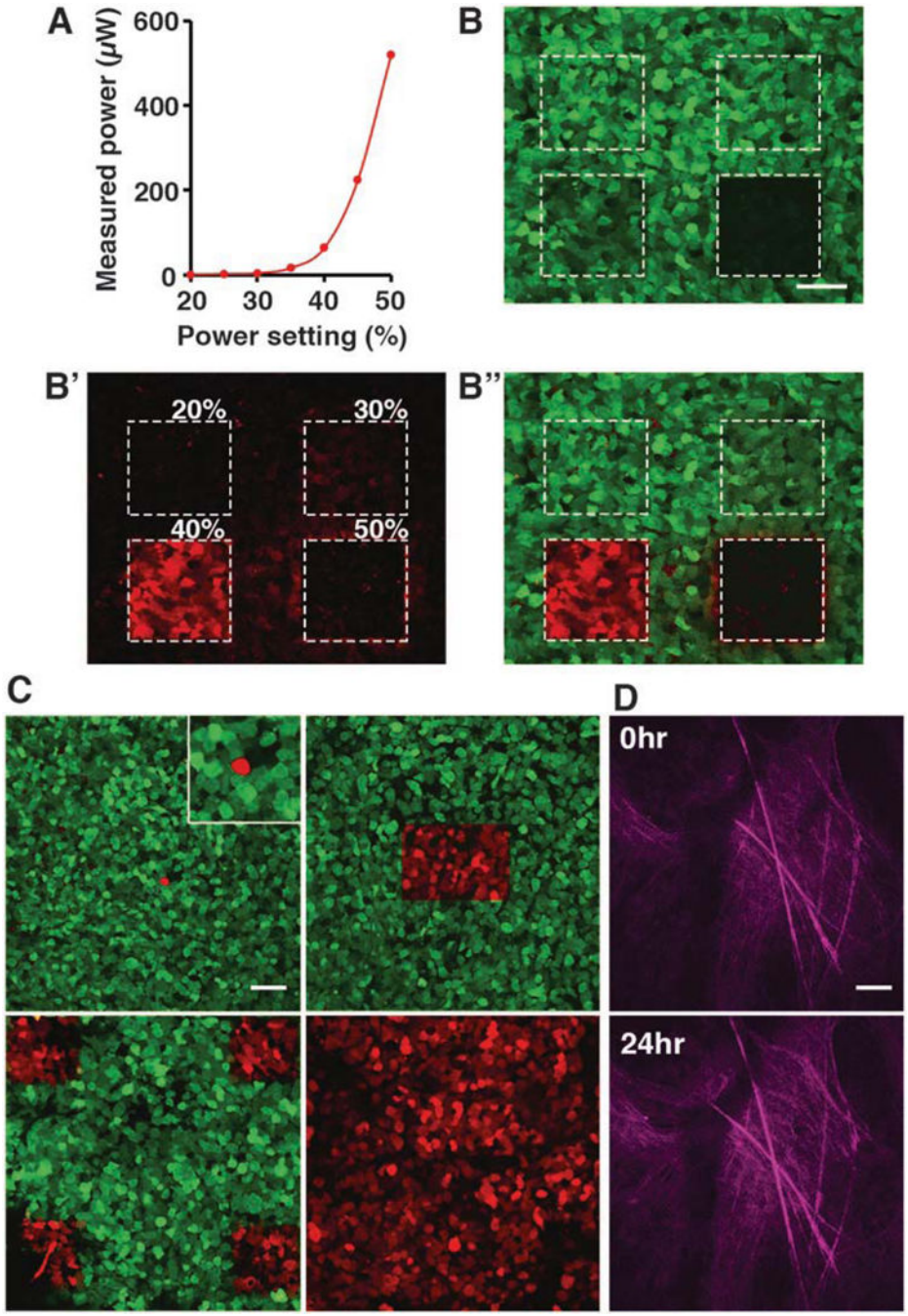

Fig. 3.

Intravital photoconversion of Dendra2-labeled tumor cells (**a**) Relationship of the 405 nm laser power setting to laser power entering the tumor tissue. Measurement was done at the focal plane of UPLSAPO 30× objective. (**b**) Photoconversion efficiency at power settings 20–50% in a MDA-MB-231-Dendra2 xenograft section. (**b**) Green channel shows the effect of photobleaching at each power setting. (**b′**) Red channel shows the emission of photoconverted red Dendra2 at each power setting. (**b″**) Merge. Scale bar 50 μm. (**c**) Photoconversion of a single cell (upper left panel, zoom in the insert), 150 × 100 μm region

containing ~100 cells (upper right panel), four 100 × 100 μm regions (lower left) and the entire FOV (lower right). Scale bar 50 μm. (**d**) Collagen fibers imaged at 0 h and relocated at 24 h using photoconverted region as a reference point. Scale bar 50 μm

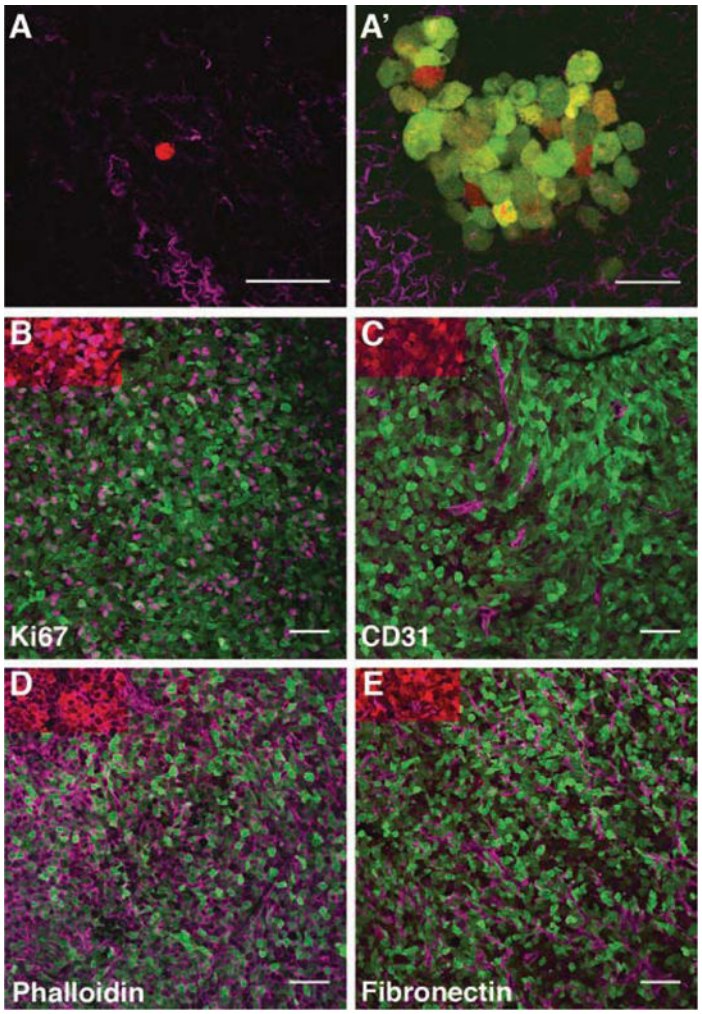

Fig. 4.

Photoconversion as a multiplexing tool: Intravital imaging and photoconversion followed by imaging of lung explants and immunofluorescence of primary tumor (**a**) Ex vivo imaging of lungs of animals imaged and photoconverted in vivo. A single photoconverted red cell in the lung (**a**) and a metastatic colony (**a′**) observed at 90 h postphotoconversion. Collagen fibers are shown in magenta. Scale bar 50 μm. The image in **a′** is reprinted with permission from [31]. (**b**–**e**) Immunofluorescence in cryosections of primary tumors imaged and photoconverted in vivo. Additional labels are shown in purple: proliferation, Ki67 (**b**), blood vessels, CD31 (**c**), actin cortex, phalloidin (**d**), ECM, fibronectin (**e**). Scale bar 50 μm